Interception of sediment-liberated phosphate in a surface aquatic system for eutrophication control

Ge Gao, Shengjiong Yang, Huining Xu, Mawuli Dzakpasu, Pengkang Jin and Xiaochang C. Wang

ABSTRACT

Phosphorus internal loading from the sediment of a surface aquatic system is considered to be the primary source of phosphorus responsible for eutrophication. In this study, we propose a possible solution to intercept phosphorus liberated from sediment to overlying water by a membranous nano-barrier (MNB) with tunable capacity. The equilibrium could be attained within 2 h when the MNB interacted with phosphate-containing water. The intercepting capacity was almost unaffected when the solution pH was varied from 4 to 10. The laboratory-scale trial showed that the MNB could positively intercept phosphorus liberated from sediment when the MNB covered the sediment, and the MNB was easy to replace once it became phosphate saturated, making its actual application feasible. Generally, the novel MNB can be considered to be a possible pathway for eutrophication control in shallow surface aquatic systems and scenic water.

Key words | barrier, eutrophication, interception, liberation, phosphate

Ge Gao
Shengjiong Yang (corresponding author)
Huining Xu
Mawuli Dzakpasu
Pengkang Jin
Xiaochang C. Wang
School of Environmental and Municipal Engineering,
Xi'an University of Architecture and Technology,
No. 13, Yanta Road, Xi'an, Shaanxi 710055,
China
E-mail: *yangshengjiong@163.com*

INTRODUCTION

Phosphorus is an essential, often limiting, nutrient element in water environments for the growth of organisms. The excessive use of phosphorus-containing products has led to significant amounts of residual phosphorus in natural aquatic systems and scenic water through agricultural and soil runoff (Zohar *et al.* 2017), manufacturing processes (Van Hoof *et al.* 2017), and discharge of effluent from municipal wastewater treatment plants (Ye *et al.* 2017). The excessive phosphorus discharged to natural aquatic systems and scenic water can accumulate and cause serious environmental problems at levels above natural thresholds. For example, excessive phosphorus can lead to eutrophication (Shin *et al.* 2017), which results in blooms of phytoplankton and cyanobacteria in aquatic systems that further cause subsequent problems, including microcystin release (Wang *et al.* 2017), death of aquatic animals, aesthetic problems, oxygen depletion, and deterioration of water quality (Worsfold *et al.* 2016). Therefore, the discharge of phosphorus has been regulated worldwide. However, eutrophication still occurs, despite some biological techniques being widely employed in municipal wastewater treatment plants to decrease the discharge of phosphorus into surface aquatic systems (Wang *et al.* 2019; Zhang *et al.* 2019). One reason that should be taken in consideration is that the phosphorus discharge standard of municipal wastewater treatment plants (0.5 mg L^{-1} in China) is higher than the threshold which initiates eutrophication (0.02 mg L^{-1}) (Bhagowati & Ahamad 2019). In addition, internal phosphorus loading (phosphorus liberated from the sediment) that replenishes phosphorus to overlying water has also been considered as the primary reason (Søndergaard *et al.* 2003). Therefore, controlling internal phosphorus loading in sediment is essential for successful relief of eutrophication.

Against this background, sediment dredging has been employed to decrease internal phosphorus loading and

doi: 10.2166/ws.2019.151

has shown considerable potential (Liu *et al.* 2016a, 2016b; Chen *et al.* 2018). Nonetheless, this method is a controversial countermeasure that is questioned because it may destroy the sediment-water interface, which is known to play a key role in stabilization of aquatic systems (Søndergaard *et al.* 2003). Furthermore, positive outcomes of nutrient control by dredging that have been reported to date were usually maintained for only short periods of time, but negative effects might last for longer periods (Ruley & Rusch 2002; Jing *et al.* 2013). Moreover, the high cost of dredging also hindered its application. Therefore, more researchers have started to search for alternative methods for eutrophication control. This has led to the development of *Phoslock®*, lanthanum modified bentonite (LMB), by Commonwealth Scientific and Industrial Research Organization (Spears *et al.* 2016). *Phoslock®* is used to cover lake sediment, which leads to the stabilization of free phosphate because of the naturally strong affinity between lanthanum and phosphate (Copetti *et al.* 2016). The stabilized phosphate is inactivated meantime and then loses its nutritional nature (Wang *et al.* 2016a). It should be stated that not only phosphate liberated from sediment is blocked, the free phosphate in overlying water is simultaneously immobilized by this method as well. It has been applied to about 200 aquatic bodies in many areas and exhibited considerable effects (Copetti *et al.* 2016). In addition, synergistic application with other techniques such as flocculation has also been attempted (Lürling & Oosterhout 2013). However, the application of this system suffers from several negative aspects. For instance, the duration of its positive effects is limited and, therefore, require frequent dosing (every 3 months; Liu *et al.* 2012) to achieve the desired efficiency (Meis *et al.* 2012). In addition, the dosage rate is calculated as 0.24–0.82 kg *Phoslock®* m^{-2} surface area of water bodies (Liu *et al.* 2012; Meis *et al.* 2012; Copetti *et al.* 2016). Dosing at this rate implies a significant increase in the total quantity of sediment due to difficulties in replacing the saturated *Phoslock®*. Furthermore, it alters the microbial ecosystem in the original sediment (the oxic-anoxic interface would be raised) by hindering the mass transfer between sediment and overlying water after it settles to the bottom (Vopel *et al.* 2008). Therefore, a replaceable *Phoslock®*-like material is desired.

In this study, a phosphate membranous nano-barrier (MNB) was developed based on La(III)-chitosan-graphene oxide. The prepared MNB was carefully characterized, and its phosphate binding performance evaluated using isotherm, kinetic, and thermodynamic study as well as the effects of initial pH, contact time, and temperature. Its performance in field applications was then evaluated in a medium-term laboratory-scale trial by using it to cover the sediment surface to intercept liberated phosphorus. In addition, the possible mechanism was also proposed.

METHODS AND MATERIALS

Development of membranous nano-barrier

Preparation of La coagulated graphene oxide composites

Graphene oxide (GO) was prepared by oxidizing natural graphite using the modified Hummers method, which was shown in SI (Guerrero-Contreras & Caballero-Briones 2015). Lanthanum-coagulated GO (La-GO) was produced by reacting GO with $LaCl_3$. Typically, GO (0.15 g) was added to 300 mL of deionized water in a 500 mL conical flask and ultrasonically dispersed for 20 min to obtain a GO dispersion. $LaCl_3$ (0.5 g) was then dissolved into the GO dispersion. The mixture was lightly stirred using a mechanical shaker for 24 h, during which time the GO was coagulated. The coagulated composites were subsequently washed with deionized water and centrifuged at 8,000 rpm (15 min) three times. La-GO was obtained after lyophilization of the solid composites.

Preparation of La loaded chitosan powder (La-CP)

Chitosan (1 g) was dissolved in 5% acetic acid by stirring with a magnetic stirrer. Next, 0.03 mol/L $LaNO_3$ solution was added to the chitosan solution at a La/chitosan ratio of 1:10 (mass proportion). The pH of the mixture was adjusted to 5.0–6.0 with aqueous ammonia (5%), then stirred for 60 minutes. Next, the mixture was precipitated by adding 25% aqueous ammonia. The precipitates were subsequently obtained, washed and dried in an air-circulating oven at 70 °C. Finally, the dried materials (La-CP) were

smashed to give a particle size lower than 100 μm for subsequent use.

Preparation of MNB

Chitosan (1.5 g) and acetic acid (2 mL) were dissolved and mixed with deionized water (100 mL) in a thermostat at 50 °C, after which the residual solid was removed and the solution was marked as S1. Next, 5 g of polyvinyl alcohol (PVA) was dissolved with deionized water (100 mL) in a thermostat at 80 °C, after which the residual solid was removed and the solution was marked as S2. Sodium alginate (2 g) was dissolved in deionized water (100 mL) in a thermostat at 50 °C, and the obtained solution was marked as S3.

S1 (50 mL) and S2 (50 mL) were mixed, after which 2 mL polyethylene glycols was added to the mixture and stirred with a magnetic stirrer for 30 min. Next, La-GO (0.15 and 0.3 g) and La-CP (1.5 g) were added to the mixture and dispersed completely. S3 (50 mL) was then slowly added to the mixed dispersion liquid and stirred at 100 rpm using a magnetic stirrer for 10 minutes. Finally, the $MNB_{0.15}$, and $MNB_{0.3}$ (subscript represents the La-GO dosage during the preparation process) were obtained by lyophilizing the final mixture.

Evaluation of phosphorus binding capacity of MNB

Isotherm studies were conducted using 25 mL of 5, 10, 15, 20, 25, and 30 mg L^{-1} of each phosphate solution and 0.2 g of MNB to evaluate the maximum phosphate removal capacity of the MNB. All the experiments were conducted at room temperature (25 ± 1 °C). The solution pH was adjusted to 6.8 ± 0.1 by 0.1 mol L^{-1} HCl or NaOH solution. The phosphate concentrations were determined after 24 h.

Phosphate solutions with an initial concentration of 20 mg L^{-1} (25 mL) were added to 11 beakers with 0.2 g MNB. 0.1 mol L^{-1} HCl or NaOH solution was added to adjust the initial solution pH to 2–12, respectively, to evaluate the pH effect. The concentration of phosphate was determined after 24 h.

Additionally, 0.2 g MNB was added to several beakers containing 50 mL of phosphate solution at 20 mg L^{-1} (pH 6.8 ± 0.1) to elucidate the kinetics and the effect of contact time. The concentration of phosphate in different beakers was then determined at different intervals (15, 30, 60, 90, 120, 150, and 180 minutes).

Laboratory-scale trial

A medium-term laboratory-scale trial was established to simulate the continuous phosphorus liberation process from sediment to overlying water. The surficial sediment sample was collected from the sediment surface (at a depth of 0–5 cm) of Xing'qing Lake, Xi'an, Shaanxi, P.R. China. Sediment was dried at 60 °C for 24 h, after which the dried sediment was smashed to reserve. Next, 200 g of smashed sediment was added into a beaker and mixed with phosphate solution (50 mg L^{-1}, 500 mL) while stirring with a magnetic stirrer for 3 days to achieve the adsorption equilibrium. The phosphorus adsorbed sediment was collected and naturally dewatered by gravity, then dried, after which it was uniformly distributed on the bottom of a glass tank to simulate the phosphorus internal sources. The phosphorus-adsorbed sediment was subsequently covered with a piece of the MNB sheet, and deionized water was added to create the sediment-overlying water system. The volume of the overlying water was replenished to 300 mL after each measurement of the phosphate concentration. In addition, a blank test was conducted to monitor the rate of phosphate liberation from sediment to overlying water by uniformly distributing phosphate-adsorbed sediment in deionized water and not applying the MNB. The overlying water in this tank was changed with deionized water after each measurement of the phosphorus concentration. The experiment was conducted continuously for more than 2 months.

Analytical method

MNB were characterized by scanning electron microscopy-energy dispersive X-ray spectroscopy (SEM-EDS, Quanta FEG 250, USA), and transmission electron microscopy (TEM, FEI Tecnai G2 F20, USA). The X-ray photoelectron spectra (XPS) were recorded through an X-ray photoelectron spectrometer (Thermo Fisher K-Alpha). The concentrations of phosphate were measured using the

ascorbic acid method (standard method 4500-P. E.) (APHA *et al.* 1999).

RESULTS AND DISCUSSION

Characteristics

The permeate flux of the MNB should be sufficient to ensure effective mass transfer between the two sides of the MNB (sediment and overlying water), which means the porosity of the MNB must be well developed. As shown in Figure 1, the surface observation of the MNB was characterized by scanning electron microscopy (SEM) and high-resolution transmission electron microscopy (HRTEM). The results revealed that the porous structure was well developed in the MNB (Figure 1(a) and 1(b)), which resulted in a large specific surface area and further uniform distribution of La-GO and La-CP in the MNB. These characteristics resulted in a greater chance for interaction between phosphate in solution and valid La sites in the MNB. Figure 1(c) and 1(d) show the HRTEM images of the MNB. An amorphous structure was observed upon analysis of the pristine MNB. However, regular crystal structures were observed after the MNB was used for phosphate binding (Figure 1(e)). Moreover, the fast Fourier transform (FFT) pattern (Figure 1(f)) obtained from Figure 1(e) showed several lattice spacings of the formed crystals. Line scan of the HRTEM image of the used MNB exhibited a minimum lattice spacing of 0.167 nm (Figure 1(g), corresponding

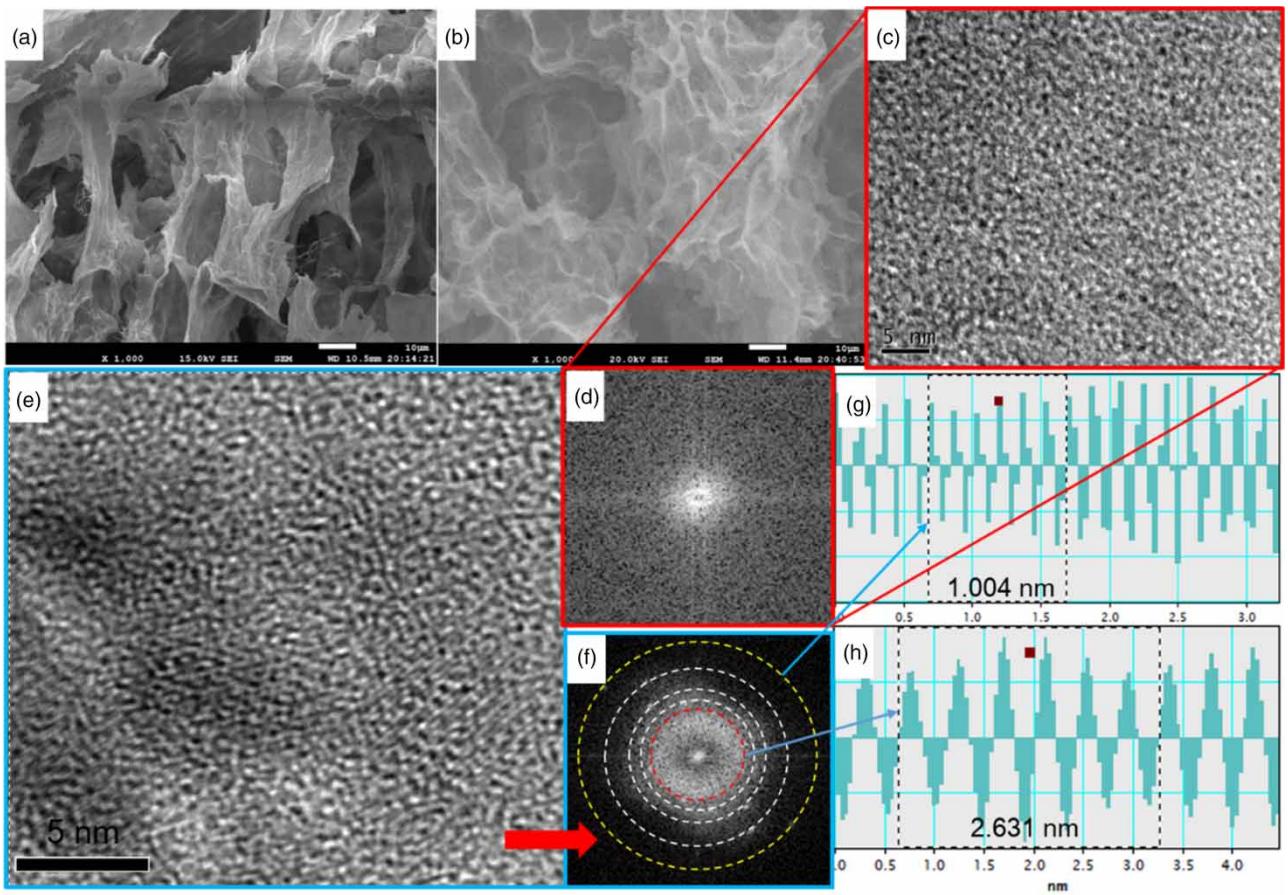

Figure 1 | Characteristics of MNB before and after phosphate binding: (a) SEM image of MNB; (b) SEM image of the used MNB; (c) HRTEM image of MNB and (d) FFT pattern obtained from (c); (e) HRTEM image of the used MNB and (f) FFT pattern obtained from (e); (g) line scan of the HRTEM image indicated by the yellow ring in (f), indicating a lattice fringe spacing of 0.167 nm, corresponding to (311) plane of $LaPO_4$ (PDF#4-635); (h) line scan of the HRTEM image indicated by the red ring in (f), indicating a lattice fringe spacing of 0.438 nm, corresponding to (101) plane of $LaPO_4$ (PDF#4-635). Please refer to the online version of this paper to see this figure in colour: http://dx.doi.org/10.2166/ws.2019.151.

to (311) plane of $LaPO_4$) and the maximum lattice spacing is 0.438 nm (Figure 1(h), corresponding to (101) plane of $LaPO_4$), indicating the lattice spacing of formed crystal is ranged between 0.167–0.438 nm, which agrees with the results reported for $LaPO_4$ nanorods/crystals (Brown *et al.* 2005; Pan *et al.* 2015). The detailed parameters of lattice spacing are shown in Figure S1 (Supporting Information).

The results of XPS analysis are shown in Figure 2. It can be seen that the P 2p peak appeared in the XPS survey of the used MNB, which was absent in the pristine MNB (Figure 2(a)), indicating considerable phosphate existed in the used MNB. The C 1 s XPS envelope of the pristine MNB (Figure 2(b)) was able to be fitted to five components at 284.4, 285.5, 286.7 and 288.2 eV, corresponding to C = C/C-C in aromatic rings, C-OH, epoxy C-O-C and C = O groups, respectively (Shao *et al.* 2016). The La 3d in the XPS spectrum of the pristine MNB (Figure 2(c)) showed two sets of peaks at 835.4 and 852.9 eV, similar to those reported for the La-OH bond (Sunding *et al.* 2011). The P 2p of the used MNB (Figure 2(d)) contained a peak at 132.9 eV that corresponds to the pentavalent P of $LaPO_4$ reported by Sissel *et al.* (Jørgensen *et al.* 2002). The C 1 s spectrum for the used MNB (Figure 2(e)) was also separated into four peaks centered at 284.1 (C = C/C-C), 285.6 (C-OH), 286.7 (epoxy C-O-C) and 288.2 eV (C = O), indicating that the phosphate binding process might cause binding energy shifting of C = C/C-C groups. The La 3d spectrum of the used MNB (Figure 2(f)) also produced two sets of peaks at 836.3 and 852.6 eV, which were similar to the values reported for $LaPO_4$ (Koilraj & Sasaki 2017). In summary, phosphate generally exists in the form of $LaPO_4$ in the MNB after phosphate binding.

Evaluation of the binding capacity

PVA and chitosan were employed to create the framework structure, but this framework structure was incapable of binding phosphorus. Therefore, La-GO and La-CP were loaded in the framework structure as functional materials to activate the phosphorus binding capacity of the resulting MNB.

Langmuir and Freundlich models was employed to obtain detailed information regarding the phosphate binding capacity by La-GO, La-CP, and MNB (Chung *et al.* 2015).

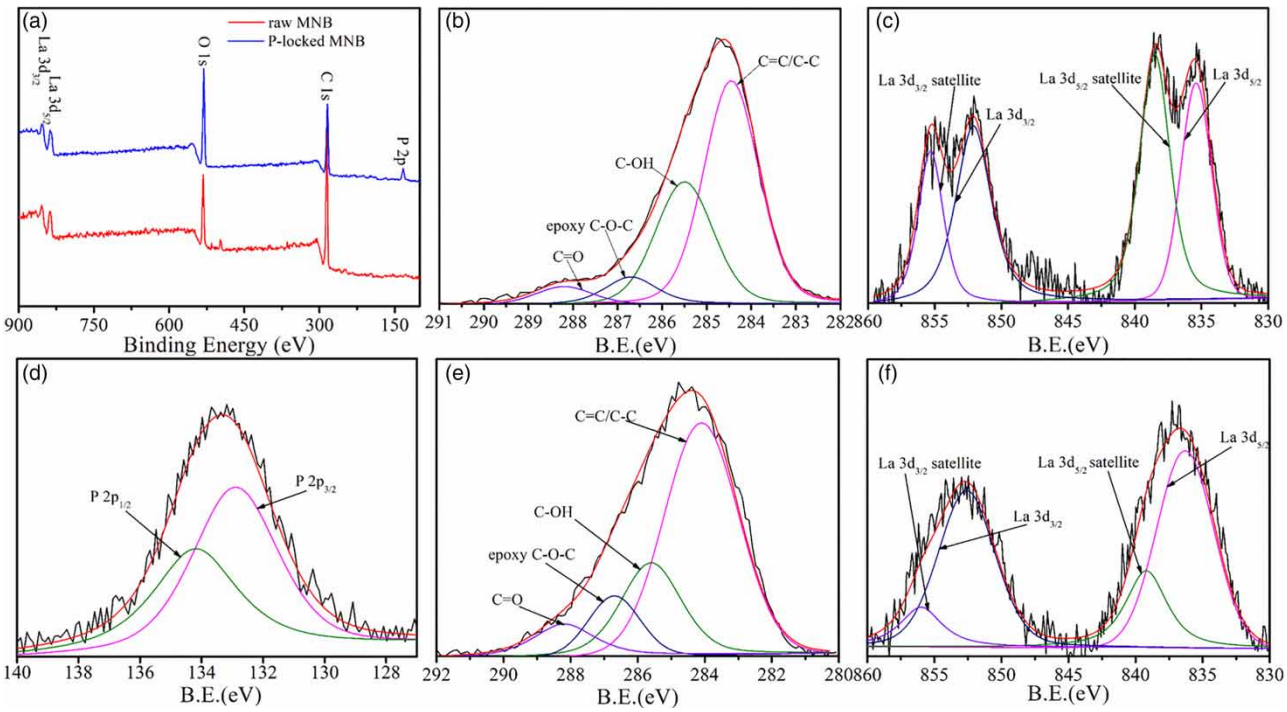

Figure 2 | XPS analysis of the pristine and used MNB: (a) XPS survey, (b) C 1 s of MNB, (c) La 3d of MNB, (d) P 2p of the used MNB, (e) C 1 s of the used MNB, and (f) La 3d of the used MNB.

The results and the corresponding parameters of the isotherm fittings are given in Table S1 (Supporting Information). It can be seen that the maximum binding capacities for phosphate to La-GO and La-CP are 141.38 mg g^{-1} and 32.36 mg g^{-1}, respectively, which is much larger than that of most other materials, such as ferrihydrite-humic acid (22.17 mg g^{-1}) (Yan *et al.* 2016) and Fe-loaded ceramic (18.48 mg g^{-1}) (Wang *et al.* 2016b), and is several times larger than that of traditional *Phoslock®*, indicates an excellent capacity for phosphate removal (Meis *et al.* 2012). Therefore, La-GO and La-CP are suitable for use as functional material for MNB development. The isotherm results of phosphate binding to MNB are also shown in Table S1. However, the results differed greatly from those observed for La-GO. The phosphate binding by MNB matched the Freundlich model better than the Langmuir model, indicating the presence of heterogeneous mechanisms with several adsorption energetic distributions in phosphate binding by MNB. In addition, the estimated maximum binding capacity for phosphate to $MNB_{0.3}$ obtained from the Langmuir model was 10.58 mg g^{-1}, which is far lower than that of La-GO and La-CP. It could be easily explained that the phosphate binding capacity depends on the mass proportion of La-GO and La-CP in MNB, further indicating that the binding capacity of the MNB is tunable by adjusting the mass proportion of La-GO and La-CP during the process of MNB synthesis (Table S1, a maximum binding capacity of 19.13 mg g^{-1} was achieved by $MNB_{0.4}$). Although the phosphate binding capacity of MNB was much lower than that of La-GO, based on its tunable capacity, it is still desirable for use as a phosphate ion barrier.

Kinetics and thermodynamics

The effect of contact time showed that the phosphate binding capacity by La-GO could be divided into a rapid stage and an equilibrium stage (Figure S2, Supporting Information). More than 90% of the binding process was finished in the rapid stage within 120 min, indicating that phosphate binding by La-GO is rapid because of the strong chemical potential in the system. However, the results differed greatly from those for the MNB.

The most useful model for describing activated chemical adsorption onto a solid surface is the Elovich equation, which is as follows:

$$q_t = \frac{1}{b}\ln(ab) + \frac{1}{b}\ln t \quad (1)$$

where a is the initial sorption rate (mg/(g min)), b is related to the extent of surface coverage and activation energy for chemisorption (g/mg), t is the contact time (min), and q_t is the amount of phosphate intercepted per gram of MNB at time t (mg g^{-1}).

Figure 3 exhibits the kinetic fitting and effect of contact time of phosphate binding by $MNB_{0.15}$ and $MNB_{0.3}$. The

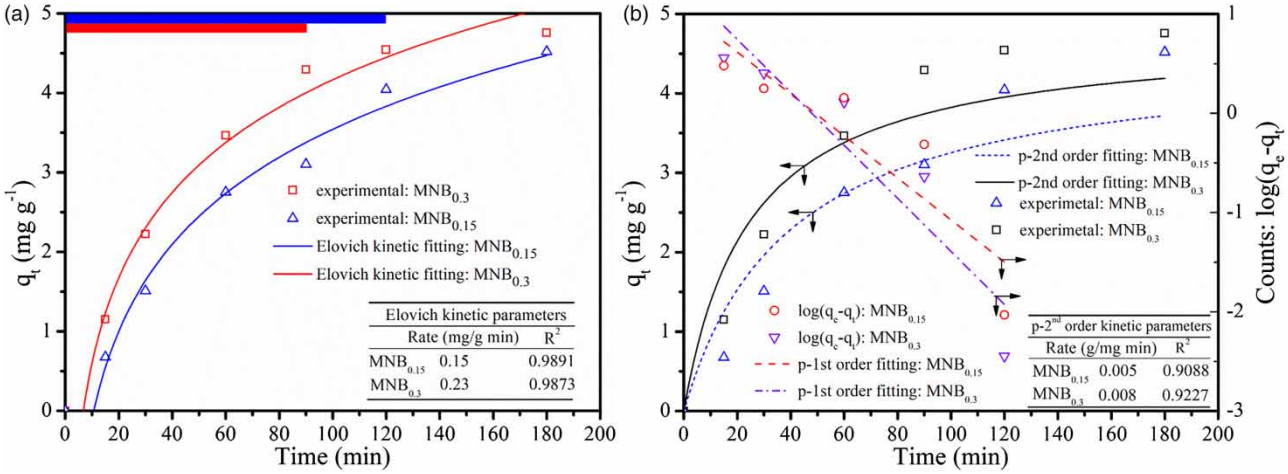

Figure 3 | Kinetics and effect of contact time of phosphate binding by MNB, (a) Elovich fitting and (b) pseudo-1st/2nd order fitting. Please refer to the online version of this paper to see this figure in colour: http://dx.doi.org/10.2166/ws.2019.151.

results showed a rare tendency to describe the effects of contact time on phosphate binding by the MNB. About 91.33% and 90.31% (in average) of phosphate binding was achieved (rapid binding stage: marked in red and blue in Figure 3(a)) within 120 and 90 minutes when $MNB_{0.15}$ and $MNB_{0.3}$ was employed, respectively, which is slower than the existing *Phoslock®* (30–40 min) (Haghseresht *et al.* 2009). In addition, the duration of the rapid binding stage is different with the difference in the mass ratio of La-GO in MNB. The experimental data were fitted to the Elovich kinetic (Figure 3(a)) and pseudo-first/second order (Figure 3(b)) kinetic models. It also could be seen that the kinetic analysis of $MNB_{0.15}$ and $MNB_{0.3}$ fitted the Elovich model very well with the initial sorption rate of 0.15 and 0.23 mg/(g min), respectively. This observation might be caused by the different amount of functional sites on the surface of different MNB, indicating that surface adsorption is more efficient when the mass ratio of La-GO is increased when preparing MNB. The Elovich kinetic model always describes reactions involving chemical adsorption onto a solid surface without desorption of adsorbate, in which the rate decreases with time because of an increase in surface coverage (Wu *et al.* 2009). Therefore, phosphate binding by MNB can be considered as a chemical adsorption process. The adsorption rate by MNB was far lower than that of La-GO, indicating that the most functional La site in MNB is covered by organic polymers. Most of the phosphate ions should diffuse into MNB, then be locked.

The effect of temperature was evaluated by Gibbs free energy change (ΔG), enthalpy change (ΔH), and entropy change (ΔS). These parameters could be estimated using equilibrium changing with different temperatures in the equations, which is exhibited in SI. The obtained parameter is shown in Table 1. The negative value of ΔG indicated the spontaneity of the binding of phosphate ions. The positive value of ΔH implied the binding of phosphate by the $MNB_{0.3}$ is endothermic in nature. The positive ΔS suggested an increased randomness at the $MNB_{0.3}$/phosphate interface during the binding process. Generally, phosphate binding by MNB was spontaneous, and higher temperature was favorable.

Table 1 | Thermodynamic parameters for the phosphate interception onto MNB

T (K)	ΔG (kJ mol^{-1})	ΔH (kJ mol^{-1})	ΔS (J mol^{-1})
293	−2.14	4.58	16.47
298	−3.07		
303	−3.5		

Effect of pH

It is well known that the phosphate dissociation equilibrium in an aqueous solution is pH dependent. This equilibrium can be described by the following equations (Figure 4):

$$H_3PO_4 \leftrightarrow H_2PO_4^- + H^+ \text{pH} < 5 \quad (2)$$

$$H_2PO_4^- \leftrightarrow HPO_4^{2-} + H^+ \; 5 < \text{pH} < 10 \quad (3)$$

$$HPO_4^{2-} \leftrightarrow PO_4^{3-} + H^+ \text{pH} > 10 \quad (4)$$

The effects of initial solution pH on phosphate binding by MNB (taking $MNB_{0.3}$ as the example) are shown in Figure 4. The phosphate binding capacity of the MNB was comparatively stable under neutral conditions. However, highly acidic and basic conditions could profoundly impact the phosphate binding capacity, leading to a reduction under extreme pH conditions.

In solutions with a low initial pH (pH < 4), phosphate mainly exists as H_3PO_4 and $H_2PO_4^-$. The $H_2PO_4^-$ in the system was removed by vacant La sites in MNB, which were kept by La-GO and La-CP. H_3PO_4 is comparatively difficult to remove by MNB because H_3PO_4 is not freely available in the binding process, and it could be removed when the phosphate dissociation equilibrium moved to $H_2PO_4^-$ (Equation (2)) because of a decreased concentration of $H_2PO_4^-$ via La affinity. As shown in the XPS analysis, La-OH bonds existed on the surface of the MNB, indicating that the mechanism might be activated as described from Equations (5)–(7). The protonation of surface hydroxyls occurred in acidic conditions, rendering a positively-charged surface, which is functional during phosphate binding via electrostatic interaction (Equation (5)). The protons were consumed during the process, which explained the pH increase after equilibrium. For solutions with an initial pH of 4–10, the phosphate binding capacity is desirable, indicating that $H_2PO_4^-$ and HPO_4^{2-} could be easily removed by MNB. The $H_2PO_4^-$ and HPO_4^{2-} were locked through inner-sphere monodentate (Equation (6)) and bidentate (Equation (7)) ligand ion exchange. H^+ was released during the process;

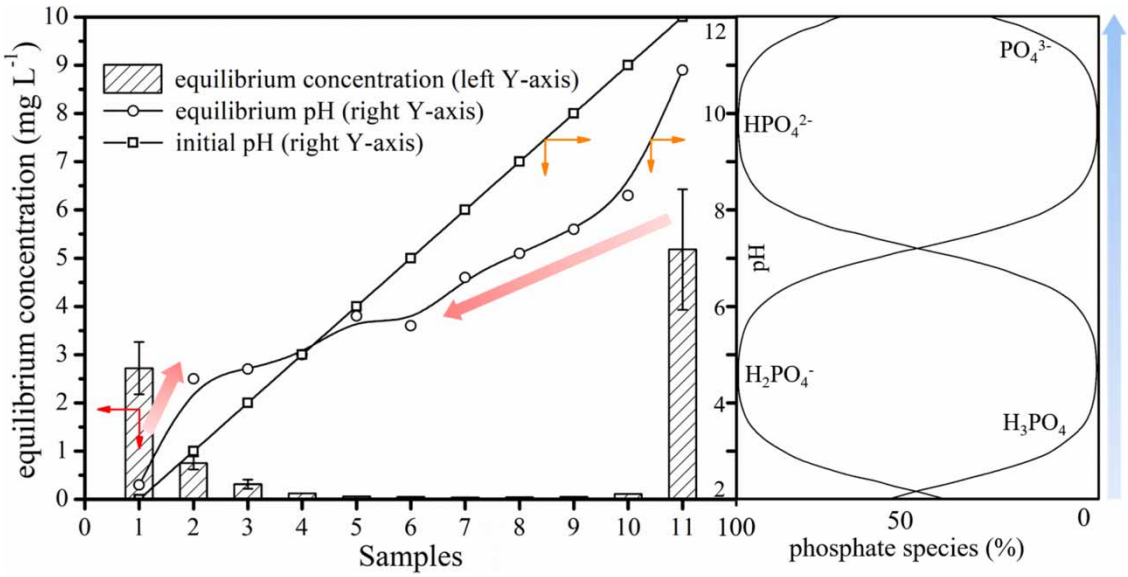

Figure 4 | Effect of initial solution pH and distribution diagram for phosphate present as different protonated species as a function of pH.

hence, the pH decreased after equilibrium. For alkaline solutions (pH > 10), the predominant phosphate species was PO_4^{3-}, which could still be easily removed by the MNB (via inner-sphere ligand ion exchange: monodentate and bidentate)

$$\equiv La \xrightarrow{H_2O \leftrightarrow H^+ + OH^-} \equiv La - OH + H \xrightarrow[\text{protonation}]{H_xPO_4^{(x-3)-}} \equiv La - OH_2^+ \cdots O - \overset{\overset{OR}{|}}{\underset{\underset{O}{|}}{P}} - OR \quad (5)$$

$$\equiv La \xrightarrow{H_2O \leftrightarrow H^+ + OH^-} \equiv La - OH \xrightarrow{H_xPO_4^{(x-3)-}} \equiv La - O - \overset{\overset{OR}{|}}{\underset{\underset{O}{|}}{P}} - OR + H^+ \quad (6)$$

$$\equiv La \xrightarrow{H_2O \leftrightarrow H^+ + OH^-} \begin{matrix} \equiv La - OH \\ \equiv La - OH \end{matrix} \xrightarrow{H_xPO_4^{(x-3)-}} \begin{matrix} \equiv La - O \\ \equiv La - O \end{matrix} \overset{\overset{OR}{|}}{\underset{\underset{OR}{|}}{P}} + H^+ \quad (7)$$

where x = 0, 1 and 2 to describe PO_4^{3-}, HPO_4^{2-}, and $H_2PO_4^-$ under different pH conditions.

However, it could be observed that the binding capacity began to decrease when the initial pH was higher than 11, and sharply decreased when the initial pH was 12. This phenomenon is possibly caused by the presence of a large amount of OH^- in alkaline solution. The high concentration of OH^- in solution activated deprotonation and further rendered a negative change of the MNB surface. The negatively charged surface is not able to bind phosphate because of the electrostatic repulsion. In addition, the strong alkaline condition might destroy the surface structure of the MNB, leading to a decrease in functional binding sites in MNB.

The reusability of the spent MNB, evaluated by base elution, demonstrated that the spent MNB could hardly be recovered due to the high chemical stability of the final products formed by -La^{3+} and phosphate (Kasprzyk *et al.* 2018). However, the La-coagulated GO solution demonstrated a high capability to significantly recover the spent MNB, mainly due to the strong contact between the porous structure of MNB and La-GO to significantly increase the creation of new functional sites on its surface. Nonetheless, complete and frequent regeneration of the spent MNB cannot be attained, whereby about only 71% (7.44 mg g^{-1}) of the removal capacity could be achieved in the second run.

Generally, the phosphate binding capacity of the MNB is desirable at pH values of 4–10. Extreme acidic and basic conditions should be avoided.

Laboratory-scale trial

A laboratory-scale trial was conducted to evaluate the feasibility and capacity of MNB for internal phosphate interception. The phosphorus adsorption capacity of the obtained sediment is shown in Figure S3 (Supporting Information). The phosphorus-saturated sediment was set in tanks as internal phosphorus sources with (labeled as E1) and without covering the MNB (labeled as E2). After more than 2 months, desirable results were obtained. As shown in Figure 5(a), the

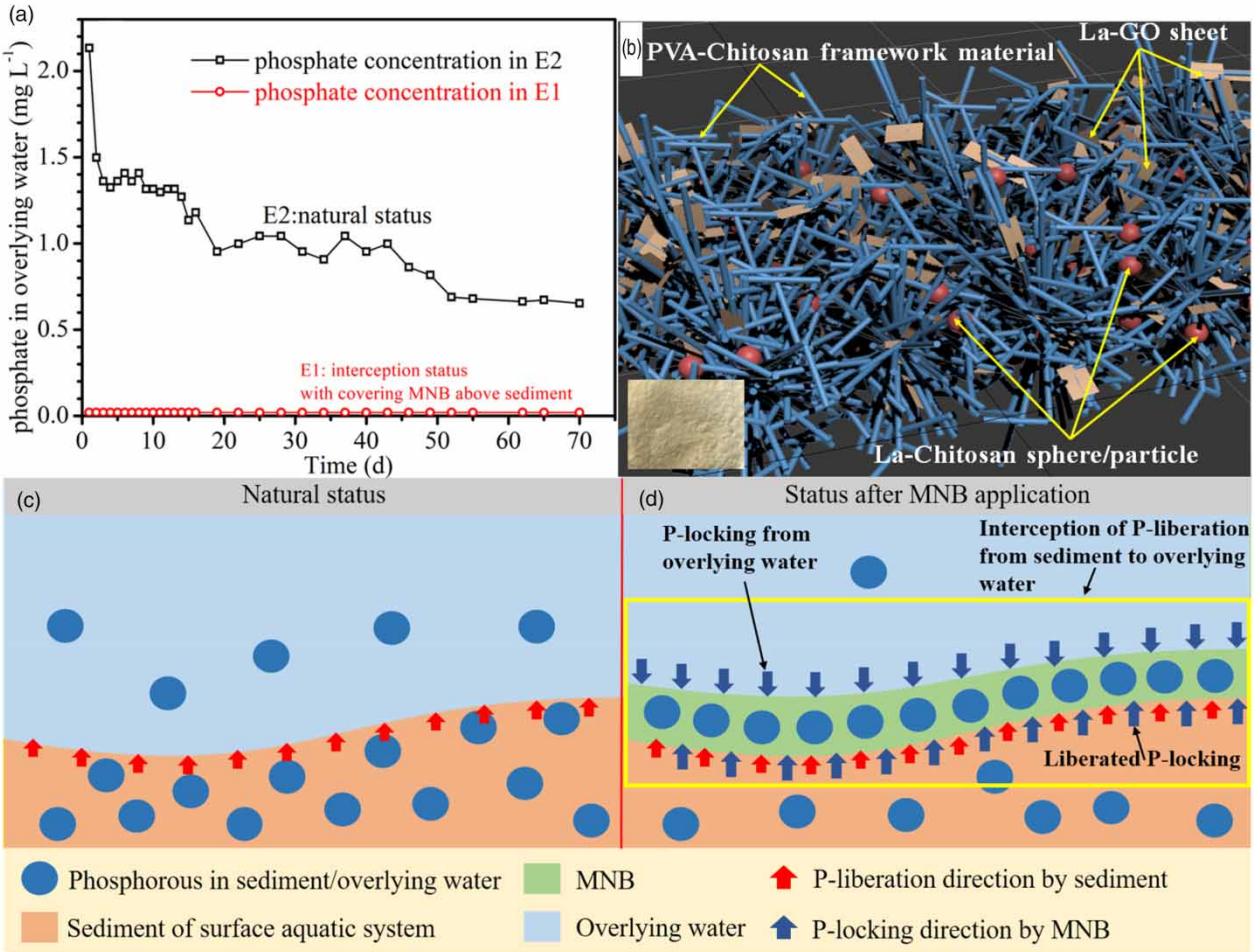

Figure 5 | (a) The performance of phosphate interception by covering MNB; (b) schematic diagram of MNB structure; (b-inset) photograph of the pristine MNB; (c) the natural status of phosphate liberation in a surface aquatic system; and (d) interception status of phosphate liberation by MNB.

phosphate concentration in the overlying water achieved 2.13 mg L^{-1} in E2 on the first day, then continuously decreased with time. The concentration in E2 decreased to 0.68 mg L^{-1} and stabilized. It can be explained by Fick's law, the mass in the high concentration phase (sediment) always tended to diffuse to the low concentration phase (overlying water), indicating that phosphate would be continuously released from sediment to the aqueous phase as an internal pollutant. As expected, different results were obtained in E1, where the phosphate concentration in the overlying water was almost too low to detect throughout the experimental period (lower than 0.005 mg L^{-1}), indicating that phosphate liberated from sediment was all locked by the MNB.

The pore structure was well developed in the MNB (Figures 1(a) and 5(b)); hence, there was considerable permeate flux for mass exchange between the sediment and overlying water, but this hindered phosphate liberation to the overlying water. As shown in Figure 5(c), phosphate liberated from sediment could easily move to the overlying water and aggravate the algal growth to induce eutrophication. While the MNB was covering the sediment as shown in Figure 5(d), the phosphate released from the sediment was locked by the MNB instead of being released to the overlying water. The holistic MNB served as a phosphate anion sieve/barrier that intercepted phosphate when it was flowing through the MNB.

The photograph of the pristine MNB (inset in Figure 5(b)) showed the membraniform shape. A demonstration experiment showed that the MNB can be easily used to partially cover the sediment surface (Figure S4, Supporting Information). Moreover, the experiment also

Table 2 | Comparison of *Phoslock*® and *Phoslock*®-like materials

Materials	Capacity (mg g^{-1})	Shape	Replaceability	Reference
Phoslock® (LMB)	9.5	powder	×	Haghseresht *et al.* (2009)
Phoslock® (LMB)	9.8	powder	×	Zamparas *et al.* (2015)
NT-25La (LMB)	14	powder	×	Kuroki *et al.* (2014)
La-AC fiber	15.3	granule	×	Zhang *et al.* (2012)
La-MCM-41	23.78	particle	×	Yang *et al.* (2011)
La-silica SBA-15	29.08	particle	×	Yang *et al.* (2011)
La-chelex-100	1.3–3.0	particle	×	Wu *et al.* (2007)
MNB	10.58	membraniform	√	This study

AC, activated carbon; MCM, a mesoporous material synthesized from cetyltrimethylammonium bromide; SBA, a mesoporous silica synthesized from a triblock copolymer Pluronic P123 and tetraethyl orthosilicate.

demonstrated that the MNB, with tunable phosphate binding capacity, is easily replaceable by conveniently exfoliating it from the surface of the sediment after it was phosphate saturated because of its membranous shape (Figure S4). Conversely, such exfoliation cannot be realized when using the traditional *Phoslock*® and *Phoslock*®-like materials because of their powder/particle shape (Table 2). Consequently, the total phosphorus loading in sediment can be further decreased with each replacement of the phosphate-saturated MNB. In addition, it should also be considered that the total quantity of sediment may continuously increase when frequently using *Phoslock*® after it is phosphate saturated because of the difficulty in replacing it (Liu *et al.* 2012). But a similar negative effect is absent in MNB application. Finally, significant variations in the surface and structure of MNB did not occur even after it was used for phosphate interception, indicating that the physical structure of the MNB was stable under aqueous conditions. Therefore, the resulting MNB is an enhanced *Phoslock*® because of its replaceability when applied in shallow aquatic systems. This method is possibly a promising pathway for eutrophication control that functions by intercepting and decreasing the internal phosphorus loading of shallow aquatic systems. Additional studies on the MNB and MNB-like materials should be carried out to further improve this pathway for enhanced eutrophication control.

CONCLUSION

The MNB material can be seen as an enhanced *Phoslock*® for eutrophication control by intercepting and decreasing the internal phosphorus loading. The phosphorus intercepting capacity is tunable by varying the mass ratio of the functional content. The interception capacity is stable within the wide pH range of 4–10. The phosphate binding process could be well described by the Elovich kinetic model without desorption of phosphate. More than 90% of binding process could be attained within 120 min, and higher temperature was favorable. The application of the MNB in shallow aquatic systems can gradually decrease the total amount of internal phosphorus loading in sediment and limit the phosphorus concentration in overlying water, which is positive for eutrophication control.

ACKNOWLEDGEMENTS

This research was supported by the National Natural Science Foundation of China (Grant No. 51508451) and the Natural Science Foundation of Shaanxi Province of China (Grant No. 2018JQ5140).

SUPPLEMENTARY MATERIAL

The Supplementary Material for this paper is available online at https://dx.doi.org/10.2166/ws.2019.151.

REFERENCES

APHA, AWWA & WPCF 1999 *Standard Methods for the Examination of Water and Wastewater*, 20th edn. American Public Health Association, Washington, DC, USA.

Bhagowati, B. & Ahamad, K. U. 2019 A review on lake eutrophication dynamics and recent developments in lake modeling. *Ecohydrology & Hydrobiology* **19** (1), 155–166.

Brown, S. S., Im, H.-J., Rondinone, A. J. & Dai, S. 2005 Facile, alternative synthesis of lanthanum phosphate nanocrystals by ultrasonication. *Journal of Colloid and Interface Science* **292** (1), 127–132.

Chen, M., Cui, J., Lin, J., Ding, S., Gong, M., Ren, M. & Tsang, D. C. W. 2018 Successful control of internal phosphorus loading after sediment dredging for 6 years: a field assessment using high-resolution sampling techniques. *Science of The Total Environment* **616–617**, 927–936.

Chung, H.-K., Kim, W.-H., Park, J., Cho, J., Jeong, T.-Y. & Park, P.-K. 2015 Application of Langmuir and Freundlich isotherms to predict adsorbate removal efficiency or required amount of adsorbent. *Journal of Industrial and Engineering Chemistry* **28**, 241–246.

Copetti, D., Finsterle, K., Marziali, L., Stefani, F., Tartari, G., Douglas, G., Reitzel, K., Spears, B. M., Winfield, I. J., Crosa, G., D'Haese, P., Yasseri, S. & Lürling, M. 2016 Eutrophication management in surface waters using lanthanum modified bentonite: a review. *Water Research* **97**, 162–174.

Guerrero-Contreras, J. & Caballero-Briones, F. 2015 Graphene oxide powders with different oxidation degree, prepared by synthesis variations of the Hummers method. *Materials Chemistry and Physics* **153**, 209–220.

Haghseresht, F., Wang, S. & Do, D. D. 2009 A novel lanthanum-modified bentonite, Phoslock, for phosphate removal from wastewaters. *Applied Clay Science* **46** (4), 369–375.

Jing, L. d., Wu, C. x., Liu, J. t., Wang, H. g. & Ao, H. y. 2013 The effects of dredging on nitrogen balance in sediment-water microcosms and implications to dredging projects. *Ecological Engineering* **52**, 167–174.

Jørgensen, S., Horst, J. A., Dyrlie, O., Larring, Y., Ræder, H. & Norby, T. 2002 XPS surface analyses of $LaPO_4$ ceramics prepared by precipitation with or without excess of PO_4^{3-}. *Surface and Interface Analysis* **34** (1), 306–310.

Kasprzyk, M., Obarska-Pempkowiak, H., Masi, F. & Gajewska, M. 2018 Possibilities of Phoslock® application to remove phosphorus compounds from wastewater treated in hybrid wetlands. *Ecological Engineering* **122**, 84–90.

Koilraj, P. & Sasaki, K. 2017 Selective removal of phosphate using La-porous carbon composites from aqueous solutions: batch and column studies. *Chemical Engineering Journal* **317**, 1059–1068.

Kuroki, V., Bosco, G. E., Fadini, P. S., Mozeto, A. A., Cestari, A. R. & Carvalho, W. A. 2014 Use of a La(III)-modified bentonite for effective phosphate removal from aqueous media. *Journal of Hazardous Materials* **274**, 124–131.

Liu, B., Liu, X., Yang, J., Garman, D. E. J., Zhang, K. & Zhang, H. 2012 Research and application of in-situ control technology for sediment rehabilitation in eutrophic water bodies. *Water Science and Technology* **65** (7), 1190–1199.

Liu, C., Shao, S., Shen, Q., Fan, C., Zhang, L. & Zhou, Q. 2016a Effects of riverine suspended particulate matter on the post-dredging increase in internal phosphorus loading across the sediment-water interface. *Environmental Pollution* **211**, 165–172.

Liu, C., Zhong, J., Wang, J., Zhang, L. & Fan, C. 2016b Fifteen-year study of environmental dredging effect on variation of nitrogen and phosphorus exchange across the sediment-water interface of an urban lake. *Environmental Pollution* **219**, 639–648.

Lürling, M. & Oosterhout, F. v. 2013 Controlling eutrophication by combined bloom precipitation and sediment phosphorus inactivation. *Water Research* **47** (17), 6527–6537.

Meis, S., Spears, B. M., Maberly, S. C., O'Malley, M. B. & Perkins, R. G. 2012 Sediment amendment with Phoslock® in Clatto Reservoir (Dundee, UK): investigating changes in sediment elemental composition and phosphorus fractionation. *Journal of Environmental Management* **93** (1), 185–193.

Pan, B., Luo, S., Su, W. & Wang, X. 2015 Photocatalytic CO_2 reduction with H_2O over $LaPO_4$ nanorods deposited with Pt cocatalyst. *Applied Catalysis B: Environmental* **168**, 458–464.

Ruley, J. E. & Rusch, K. A. 2002 An assessment of long-term post-restoration water quality trends in a shallow, subtropical, urban hypereutrophic lake. *Ecological Engineering* **19** (4), 265–280.

Shao, L., Li, J., Guang, Y., Zhang, Y., Zhang, H., Che, X. & Wang, Y. 2016 PVA/polyethyleneimine-functionalized graphene composites with optimized properties. *Materials & Design* **99**, 235–242.

Shin, M., Lee, H.-J., Kim, M. S., Park, N.-B. & Lee, C. 2017 Control of the red tide dinoflagellate *Cochlodinium polykrikoides* by ozone in seawater. *Water Research* **109**, 237–244.

Søndergaard, M., Jensen, J. P. & Jeppesen, E. 2003 Role of sediment and internal loading of phosphorus in shallow lakes. *Hydrobiologia* **506** (1), 135–145.

Spears, B. M., Mackay, E. B., Yasseri, S., Gunn, I. D. M., Waters, K. E., Andrews, C., Cole, S., De Ville, M., Kelly, A., Meis, S., Moore, A. L., Nürnberg, G. K., van Oosterhout, F., Pitt, J.-A., Madgwick, G., Woods, H. J. & Lürling, M. 2016 A meta-analysis of water quality and aquatic macrophyte responses in 18 lakes treated with lanthanum modified bentonite (Phoslock®). *Water Research* **97**, 111–121.

Sunding, M. F., Hadidi, K., Diplas, S., Løvvik, O. M., Norby, T. E. & Gunnæs, A. E. 2011 XPS characterisation of in situ treated lanthanum oxide and hydroxide using tailored charge referencing and peak fitting procedures. *Journal of Electron Spectroscopy and Related Phenomena* **184** (7), 399–409.

Van Hoof, G., Fan, M. & Lievens, A. 2017 Use of product and ingredient tools to assess the environmental profile of automatic dishwashing detergents. *Journal of Cleaner Production* **142**, 3536–3543.

Vopel, K., Gibbs, M., Hickey, C. W. & Quinn, J. 2008 Modification of sediment water solute exchange by sediment-capping materials: effects on O_2 and pH. *Marine and Freshwater Research* **59** (12), 1101–1110.

Wang, C., Bai, L., Jiang, H.-L. & Xu, H. 2016a Algal bloom sedimentation induces variable control of lake eutrophication by phosphorus inactivating agents. *Science of The Total Environment* **557–558**, 479–488.

Wang, D., Chen, N., Yu, Y., Hu, W. & Feng, C. 2016b Investigation on the adsorption of phosphorus by Fe-loaded ceramic adsorbent. *Journal of Colloid and Interface Science* **464**, 277–284.

Wang, Z., Zhang, J., Li, E., Zhang, L., Wang, X. & Song, L. 2017 Combined toxic effects and mechanisms of microsystin-LR and copper on Vallisneria Natans (Lour.) Hara seedlings. *Journal of Hazardous Materials* **328**, 108–116.

Wang, J., Chon, K., Ren, X., Kou, Y., Chae, K.-J. & Piao, Y. 2019 Effects of beneficial microorganisms on nutrient removal and excess sludge production in an anaerobic-anoxic/oxic (A^2O) process for municipal wastewater treatment. *Bioresource Technology* **281**, 90–98.

Worsfold, P., McKelvie, I. & Monbet, P. 2016 Determination of phosphorus in natural waters: a historical review. *Analytica Chimica Acta* **918**, 8–20.

Wu, R. S. S., Lam, K. H., Lee, J. M. N. & Lau, T. C. 2007 Removal of phosphate from water by a highly selective La(III)-chelex resin. *Chemosphere* **69** (2), 289–294.

Wu, F.-C., Tseng, R.-L. & Juang, R.-S. 2009 Characteristics of Elovich equation used for the analysis of adsorption kinetics in dye-chitosan systems. *Chemical Engineering Journal* **150** (2), 366–373.

Yan, J., Jiang, T., Yao, Y., Lu, S., Wang, Q. & Wei, S. 2016 Preliminary investigation of phosphorus adsorption onto two types of iron oxide-organic matter complexes. *Journal of Environmental Sciences* **42**, 152–162.

Yang, J., Zhou, L., Zhao, L., Zhang, H., Yin, J., Wei, G., Qian, K., Wang, Y. & Yu, C. 2011 A designed nanoporous material for phosphate removal with high efficiency. *Journal of Materials Chemistry* **21** (8), 2489–2494.

Ye, Y., Ngo, H. H., Guo, W., Liu, Y., Li, J., Liu, Y., Zhang, X. & Jia, H. 2017 Insight into chemical phosphate recovery from municipal wastewater. *Science of The Total Environment* **576**, 159–171.

Zamparas, M., Gavriil, G., Coutelieris, F. A. & Zacharias, I. 2015 A theoretical and experimental study on the P-adsorption capacity of Phoslock™. *Applied Surface Science* **335**, 147–152.

Zhang, L., Zhou, Q., Liu, J., Chang, N., Wan, L. & Chen, J. 2012 Phosphate adsorption on lanthanum hydroxide-doped activated carbon fiber. *Chemical Engineering Journal* **185–186**, 160–167.

Zhang, H., Feng, J., Chen, S., Zhao, Z., Li, B., Wang, Y., Jia, J., Li, S., Wang, Y., Yan, M., Lu, K. & Hao, H. 2019 Geographical patterns of nirS gene abundance and nirS-type denitrifying bacterial community associated with activated sludge from different wastewater treatment plants. *Microbial Ecology* **77** (2), 304–316.

Zohar, I., Ippolito, J. A., Massey, M. S. & Litaor, I. M. 2017 Innovative approach for recycling phosphorous from agro-wastewaters using water treatment residuals (WTR). *Chemosphere* **168**, 234–243.

First received 27 June 2019; accepted in revised form 3 October 2019. Available online 21 October 2019